第 35 卷第 4 期
2019 年 4 月

无 机 化 学 学 报
CHINESE JOURNAL OF INORGANIC CHEMISTRY

Vol.35 No.4
674-686

柚子皮衍生类蜂窝状碳材料在同步检测重金属离子中的应用

张 婷[1] 马仕杰[1] 潘 逸[1] 管继彪[1] 张 明[1] 朱 罕[2] 杜明亮*,[2]

([1] 浙江理工大学材料与纺织学院、丝绸学院,杭州 310018)

([2] 江南大学化学与材料工程学院食品胶体与生物技术教育部重点实验室,无锡 214122)

摘要: 不含金属的碳材料通过廉价且易获得的柚子皮经 KOH 活化和高温热解获得,该碳材料具有高比表面积(1 055 $m^2 \cdot g^{-1}$)和高石墨化程度的类蜂窝状结构。将多孔碳(PAC)材料修饰后的电极作为工作电极,采用阳极溶出伏安法(SWASV)同步检测 Cd^{2+}、Pb^{2+}和 Cu^{2+}离子,表现出较高的灵敏度、可重复性、稳定性和较低的检测限。研究认为 PAC 的微孔和中孔可以充当有效的离子传递通道,从而加速离子的扩散并显著提高交换效率,而高的石墨化程度提高了材料的导电性,加速了电子传输。

关键词: 碳质材料; 柚子皮; 类蜂窝状结构; 多孔材料; 重金属离子检测; 方波阳极溶出伏安法(SWASV)

中图分类号: O646 **文献标识码**: A **文章编号**: 1001-4861(2019)04-0674-13

DOI:10.11862/CJIC.2019.077

Honeycomb-like Carbon Materials Derived from Pomelo Peels for the Simultaneous Detection of Heavy Metal Ions

ZHANG Ting[1] MA Shi-Jie[1] PAN Yi[1] GUAN Ji-Biao[1] ZHANG Ming[1] ZHU Han[2] DU Ming-Liang*,[2]

([1]*College of Materials and Textiles, Zhejiang Sci-Tech University, Hangzhou* 310018, *China*)

([2]*Key Laboratory of Synthetic and Biological Colloids, Ministry of Education, School of Chemical and Material Engineering, Jiangnan University, Wuxi, Jiangsu* 214122, *China*)

Abstract: The metal-free carbon materials were obtained by a facile KOH activation and pyrolysis process from inexpensive and readily available pomelo peels, and possessed honeycomb-like nanostructures with a high specific surface area of 1 055 $m^2 \cdot g^{-1}$ and a high graphitization degree. A porous activated carbon (PAC) material modified electrode was utilized as the working electrode for the simultaneous detection of Cd^{2+}, Pb^{2+}, and Cu^{2+} using square-wave anodic stripping voltammetry (SWASV) and exhibited high sensitivity, repeatability, stability and a low detection limit. The interconnected micropores and mesopores act as efficient ion-transfer channels and provid active surface areas with high accessibility, which serve as transport highways to accelerate mass diffusion and significantly promote exchange efficiency. High graphitization degree increases the electrical conductivity of the material and accelerates electron transport.

Keywords: carbonaceous materials; pomelo peels; honeycomb-like nanostructures; porous materials; heavy metal ion detection; square-wave anodic stripping voltammetry (SWASV)

Recently, heavy metal ions have attracted broad attention due to their hard-degraded properties, high toxicity and stability[1-3]. These ions, such as Cd^{2+}, Pb^{2+} and Cu^{2+}, pose a serious threat to the environmental ecology, food safety and human health[4-5]. Therefore, it is highly necessary to develop robust and facile

收稿日期:2018-09-25。**收修改稿日期**:2019-01-22。

国家自然科学基金(No.51373154, 51573166)**资助项目**。

*通信联系人。E-mail:du@jiangnan.edu.cn

methods for heavy metal analysis with high sensitivity and efficiency.

To date, many methods, such as atomic fluorescence spectrometry (AFS)[6], inductively coupled plasma mass spectrometry (ICP-MS)[7], atomic absorption spectroscopy (AAS)[8], and X-ray fluorescence (XRF) spectrometry[9], have been applied to the detection of heavy metal ions in different areas. Generally, the simultaneous detection of heavy metal ions usually employs noble metals and complex synthetic methods, which seriously restricts their widespread use in real-time online and continuous monitoring applications[10-12]. Therefore, it is essential and crucial to explore a cheap and facile method for the simultaneous and separate detection of heavy metal ions. In the meantime, an electrochemical detection method, square-wave anodic stripping voltammetry (SWASV), has been developed with all above features and proved to be a facile, quick and high-effective method[13-16]. There are three basic steps regarding the detection of heavy ion metals using the SWASV method: (1) Cathode pre-enrichment: with constant stirring of the solution, the heavy metal ion component is electrochemically reduced to a zero valence state and is pre-enriched onto the working electrode surface; (2) Standing: a constant potential of the cathode is maintained; stirring ceases; and then the electrode surface and the solution, in which the mass transfer occurs, are steady, so a large amount of metal can be deposited on the electrode; (3) Anodic stripping: the solution is not stirred, and an anodic potential scan is applied. The zero-valence state of the heavy metals accumulated on the surface of the working electrode is oxidized and transforms back to the corresponding cations. These cations dissociate from the surface of the working electrode and enter into the solution.

Recently, carbon materials such as carbon nanotubes, carbon nanofibers, graphene, and mesoporous carbon have been widely used as the electrode materials for the hydrogen evolution reaction, oxygen evolution reaction, oxygen reduction reaction and heavy metal ion detection due to their abundance[17-20]. Additionally, carbon materials such as mesoporous carbon are also used as an electrocatalyst carrier[21]. Among them, biomass-derived mesoporous carbon materials possess many perfect characteristics such as a high specific surface area and a porous structure, and are renewable and sustainable, which suggest great potential and capability in catalysis applications[22-24]. However, the process of preparing mesoporous carbon is usually complicated and costly. To date, many activation methods, including hard-template methods, soft-template methods, physical (CO_2, NH_3 and H_2O) activation and chemical (KOH, $ZnCl_2$ and H_3PO_4) activation, produce porous carbon with high surface areas[25-29].

To date, biomass-derived materials have been used as non-toxic and metal-free precursors for carbon-based catalysts. Pomelo is a popular fruit all over the world, and its peels are an ideal precursor for biomass-derived carbon materials. Additionally, the prepared nanostructured carbon materials can be used to address energy and environmental challenges. As reported, the derived carbon materials from pomelo peels not only show excellent specific capacitance, rate capability and cyclic stability in lithium-ion batteries (LIBs) and supercapacitors but also show a considerable enhancement in the catalytic activity and stability of oxygen evolution reactions (OERs) and oxygen reduction reactions (ORRs)[30-32]. This enhancement is due to large surface areas, high mass transfer fluxes and active loading, which can provide more active sites and serve as transport pathways to accelerate mass diffusion and finally improve the exchange efficiency.

Traditionally, to realize highly sensitive and selective electroanalysis, noble metal nanoparticle decoration of an electrode is essential. It has been reported that for porous carbon materials, the interconnected hierarchical pore architecture and high graphitization facilitate electron transfer and mass transport, which help boost the electrocatalytic activity[27,33-35]. In our previous investigations, we synthesized well-dispersed noble metal nanoparticles on carbon nanofibers via electrospinning technology, followed by *in situ* thermal reduction, and the as-synthesized nanofibers with

noble metal nanoparticles exhibited excellent electroanalytical activity and sensitivity towards the detection of heavy metal ions[36]. Herein, we developed a facile strategy to synthesize honeycomb-like carbon materials with high surface areas and hierarchical pore architectures derived from pomelo peels activated with KOH, which can be used for the efficient detection of heavy metal ions[25].

1 Experimental

1.1 Preparation of PAC and UAC

A white flocculent layer was peeled from the pomelo and cut into small pieces. Then, these pieces were washed with distilled water several times and dried at a temperature of 60 ℃. The dried pomelo samples became yellow, were soaked in 1 mol·L^{-1} KOH for 10 hours and then dried. The soaked pieces were placed into a tube furnace, heated to 700 ℃ (ramp rate: 5 ℃ per minute) and maintained for 3 hours under an Ar flow atmosphere. Then, the carbonized pieces were ground into a fine powder. Finally, the prepared samples were soaked in 1 mol·L^{-1} HCl for 3 hours, then washed with distilled water several times, and dried at 60 ℃ for 5 hours. The obtained porous activated carbon material is denoted as PAC.

The unactivated carbon was processed using the same method as that of the PAC material, except the samples were soaked in KOH and HCl. This sample is referred to as UAC.

1.2 Characterizations

The morphological images of PAC and UAC were acquired using the field emission scanning electron microscopy (JSM-6700F, FESEM, JEOL, Japan) and transmission electron microscopy (JSM-2100, TEM, JEOL, Japan), acceleration voltage was 3 and 200 kV respectively. High-angle annular dark field scanning transmission electron microscopy (HAADF-STEM) images and STEM mappings were recorded using an STEM (Tecnai G2 F30S-Twin, HAADF-STEM, Philips-FEI) at an acceleration voltage of 300 kV. Crystallographic information of the prepared samples was recorded using powder X-ray diffraction patterns (XRD, Bruker AXS D8 Advance) measured with Cu $K\alpha$ radiation (wavelength of 0.154 06 nm). The scanning range was 10° to 70°, and the scanning rate was 5° per minute. The operating voltage was 40 mV and operating current was 40 mA. The X-ray photoelectron spectra of the products were recorded using an X-ray photoelectron spectrometer (Kratos Axis Ultra DLD) with an Al (mono) $K\alpha$ source (1 486.6 eV). The Al $K\alpha$ source was operated at 15 kV and 10 mA. The specific surface area was calculated using the Brunauer-Emmett-Teller (BET, 3H-2000PSI) method, and the pore size distribution data were evaluated using the Barrett-Joyner-Halenda (BJH, 3H-2000PSI) method. The Raman spectra were measured by a micro-Raman system (Thermo Fisher Scientific DXR laser Raman microscope) operating with a 532 nm wavelength laser in the wavenumber range from 1 000 to 2 000 cm^{-1} under ambient conditions.

1.3 Electrochemical analyses

A bare GCE was ultrasonically processed with ethanol and distilled water for 20 min to reduce the surface residue. Then, the electrode was polished carefully with alumina slurry, followed by washing with ethanol and doubly distilled water and then drying. 3 mg of PAC (or UAC) powder was dispersed in 1 mL of a solvent, composed of 3∶1 (*V*/*V*) isopropanol/distilled water and 25 μL Nafion solution (5% (*w*/*w*)). The solvent was mixed using ultrasonication to form a homogeneous ink. Additionally, 5 μL of the ink was carefully transferred onto the GCE and dried at room temperature. The modified electrode is denoted as PAC/GCE (or UAC/GCE). After solvent evaporation, the electrodes were stored in a desiccator at room temperature prior to further characterization.

Cyclic voltammetry (CV) and SWASV curves were measured using a CHI660E electrochemical workstation (Chenhua Instruments Co., Shanghai, China). All the electrochemical measurements were performed with a three-electrode system: a modified GCE (PAC/GCE) as the working electrode, a platinum electrode as the counter electrode and a saturated calomel electrode (SCE) as the reference electrode. CV data were acquired in a neutral solution of 5 mmol·L^{-1}

$K_3[Fe(CN)_6]$ with steps from −1.8 to 1.5 V vs SCE at a scan rate of 100 mV·s^{-1}. SWASV was used for the simultaneous detection of Cd^{2+}, Pb^{2+} and Cu^{2+} ions. Firstly, the PAC/GCE electrode was immersed into a 0.1 mol·L^{-1} of sodium acetate buffer solution with heavy metal ions. Then, the metals were deposited onto the surface of the modified electrode at a potential of −2.1 V vs SCE for 210 s. Briefly, the deposition process was realized via a reduction in the corresponding heavy metal ions in the mixture solution, followed by another invertible process: stripping. All the experiments were carried out under the following experimental conditions: the scanning potential ranged from −1.2 to 0.3 V; the amplitude was 50 mV; the increment potential was 4 mV; and the frequency was 15 Hz. Moreover, other external conditions were controlled to ensure the comparability of each experiment. A positive potential was applied to the working electrode for 60 s to remove the deposited residual species from the surface after each detection test. To obtain the maximum sensitivity and the minimum limit of detection with the modified electrode (PAC/GCE), the corresponding voltammetric parameters (deposition potential and deposition time) were optimized via repeated experiments under similar conditions.

2　Results and discussion

2.1　Morphology of the PAC materials

In the present investigations, the porous carbon material derived from the white flocculent layer of the pomelo peels were prepared using a facile activation and carbonization process. Firstly, the dried peels were pretreated with KOH and then carbonized to form a porous and graphitic nanostructure. Fig.1a and 1b show the morphological features of PAC and UAC. In Fig.1a, it can be observed that the carbon sheet of

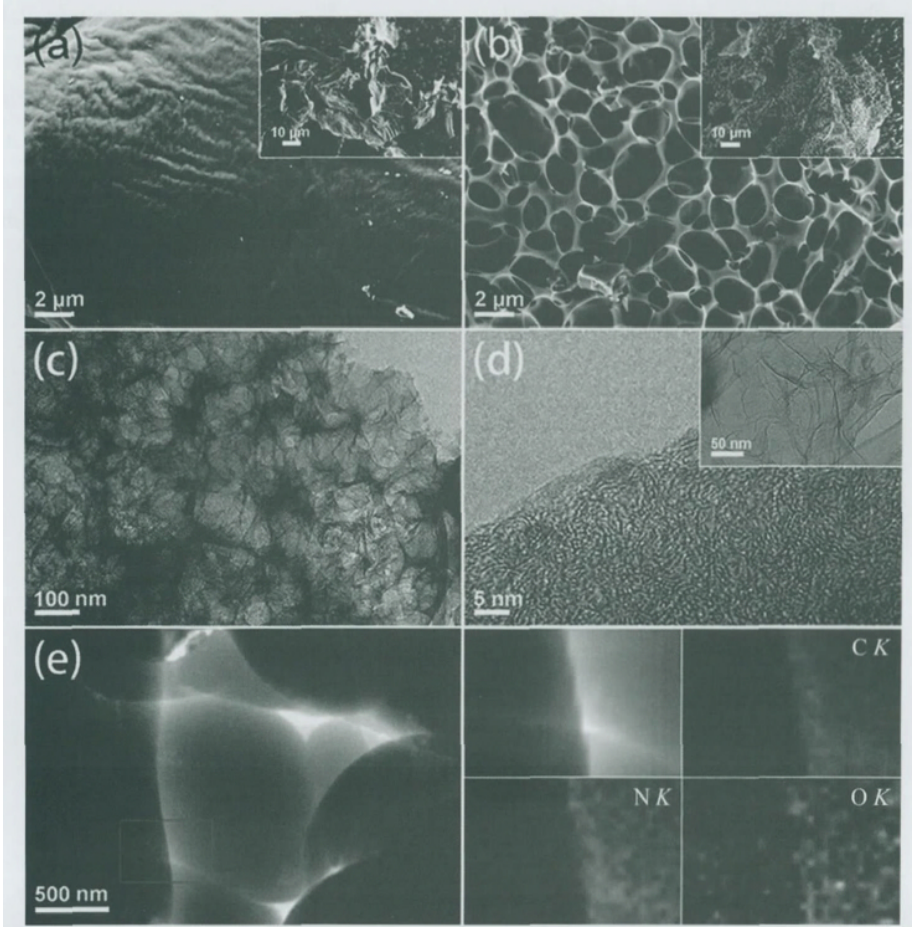

Fig.1　(a, b) SEM images of UAC and PAC; (c, d) TEM images of PAC; (e) High-angle annular dark field STEM and elemental mapping images of C, N and O in PAC

UAC was relatively smooth, and the inset in Fig.1a shows the overall morphology of UAC and demonstrates that this material was mainly comprised of large sheets. After KOH activation, the smooth sheets were broken and formed a porous honeycomb-like structure (Fig.1b). The TEM in the Fig.1c further highlighted a number of sheets exhibiting the porous honeycomb-like structures and the sheets were thin. Meanwhile, as shown in Fig.1d, the sheets were composed of turbostratic graphitic nanostructures that showed different short-range orders[37]. Obviously, it confirmed that the carbonization process at 700 ℃ in an Ar atmosphere could convert the natural flocculent layer of pomelo peels to a valuable carbon material. KOH activation at high temperature resulted in the formation of carbon materials with an interconnected hierarchical pore architecture and high graphitization. During the activation process, KOH reacted with the carbon groups in the flocculent layer of the pomelo peels to form a K_2CO_3. Then, during high-temperature calcination, the release of CO_2 molecules from the K_2CO_3 decomposition reaction caused the porous structure, and then the carbon structure was partially graphitized[25]. Therefore, the activation by KOH not only increases the specific surface area and porosity of the biomass-derived carbon materials but also enhances the degree of carbon graphitization, and both are beneficial for heavy metal detection applications. Additionally, the element mapping of atomic species (Fig.1e) clearly indicated that C, N and O were uniformly distributed in the porous carbon sheets.

2.2 Characterizations of the PAC materials

Fig.2a presents the nitrogen adsorption-desorption isotherm of PAC and determines that these isotherms were type-**Ⅳ** based on IUPAC classification. Additionally, the results indicated the formation of a honeycomb-like porous structure and a significant increase in both the specific surface area and pore volume after KOH activation, as well as high-temperature carbonization. The specific surface area was estimated to be 1 055 $m^2 \cdot g^{-1}$, and the pore diameter mainly ranged from 0 to 5 nm with an average diameter of approximately 2.19 nm. In the present investigation, the combined interconnected micropores and mesopores act as efficient ion-transfer channels and provide active surface areas with high accessibility, which serve as transport highways to accelerate mass diffusion and significantly promote the

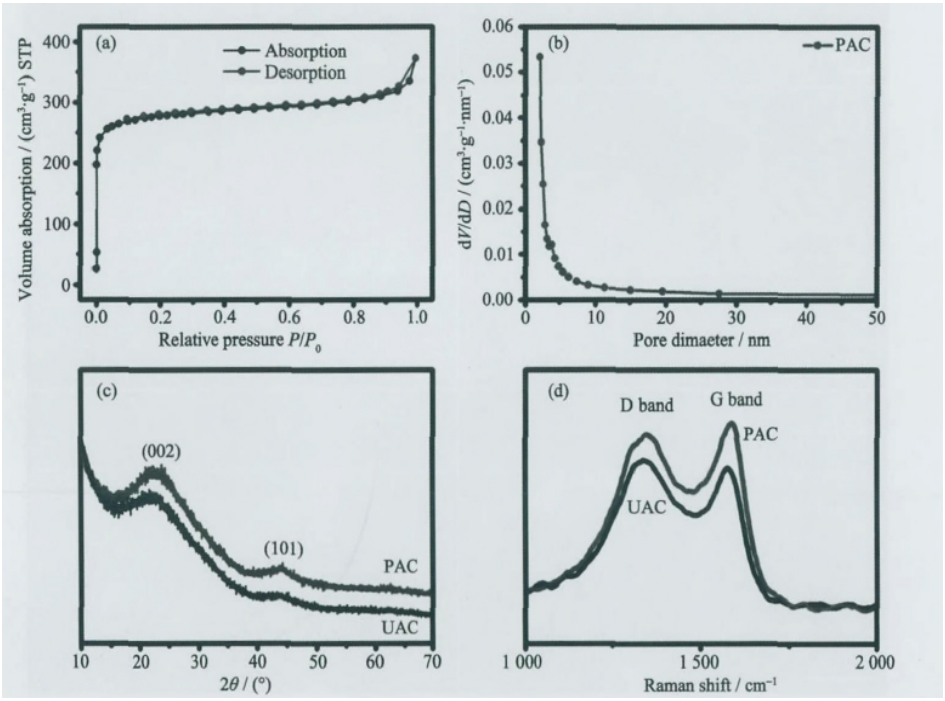

Fig.2 (a) Nitrogen adsorption-desorption isotherms of PAC; (b) Pore size distribution of PAC; (c) XRD patterns and (d) Raman spectra of UAC and PAC

exchange efficiency.

The XRD patterns and Raman spectra of UAC and PAC are shown in Fig.2c and 2d. Both UAC and PAC exhibited two broad peaks at 2θ=23° and 43° that were assigned to the (002) and (101) planes, respectively, corresponding to a graphitic carbon structure. The XRD results suggested that the (002) peak of PAC shifted to a higher angle compared with that of UAC, indicating a narrower *d*-spacing. Moreover, the (101) peak of PAC became sharper, demonstrating a higher graphitization of the porous carbon materials after KOH activation. As is well known, complete graphitization occurs at extremely high temperatures. The above results indicate that high-temperature calcination after the activation process stimulates the formation of the graphitic carbon structure, which can enhance the conductivity and benefit ion transfer. Meanwhile, as shown in Fig.2d, UAC and PAC both exhibited two broad characteristic peaks centered at 1 335 and 1 585 cm^{-1}. The peak at 1 335 cm^{-1} was ascribed to disorder-induced carbon (D band, amorphous carbon structure) that is induced by sp^3-bonded carbon atoms, while that at 1 580 cm^{-1} was ascribed to graphite in-plane vibrations (G band, graphitic carbon structure) induced by sp^2-bonded carbon atoms in a two-dimensional hexagonal graphitic layer[38]. Moreover, the peak intensity ratios of D band to G band (I_D/I_G) for UAC and PAC are 1.05 and 0.85, respectively, which further proves that KOH activation helps improve the degree of graphitization and also tally with the above XRD results.

The chemical composition and electronic structures of the PAC samples were further investigated by XPS (Fig.3). Fig.3a shows the characteristic O1*s*, N1*s* and C1*s* peaks at binding energy of 284.8, 400.31 and 532.53 eV, respectively. To deeply illustrate the electronic structures of the atomic species, the species and chemical states of C, N and O were displayed in Fig.3(b~d). As shown in Fig.3b, the spectrum of PAC was fitted by three peaks with binding energies at approximately 284.7 eV (C-C, C=C, C-N), 285.6 eV (C-O, C=O, C-OH) and 287.8 eV (O=C-C, O=C-N). The deconvoluted N1*s* peak in Fig. 3c showed four well-resolved peaks at 398.68, 400.20, 401.02 and 402.30 eV, assigning to pyridinic, pyrrolic, graphitic and oxidized nitrogen species, respectively.

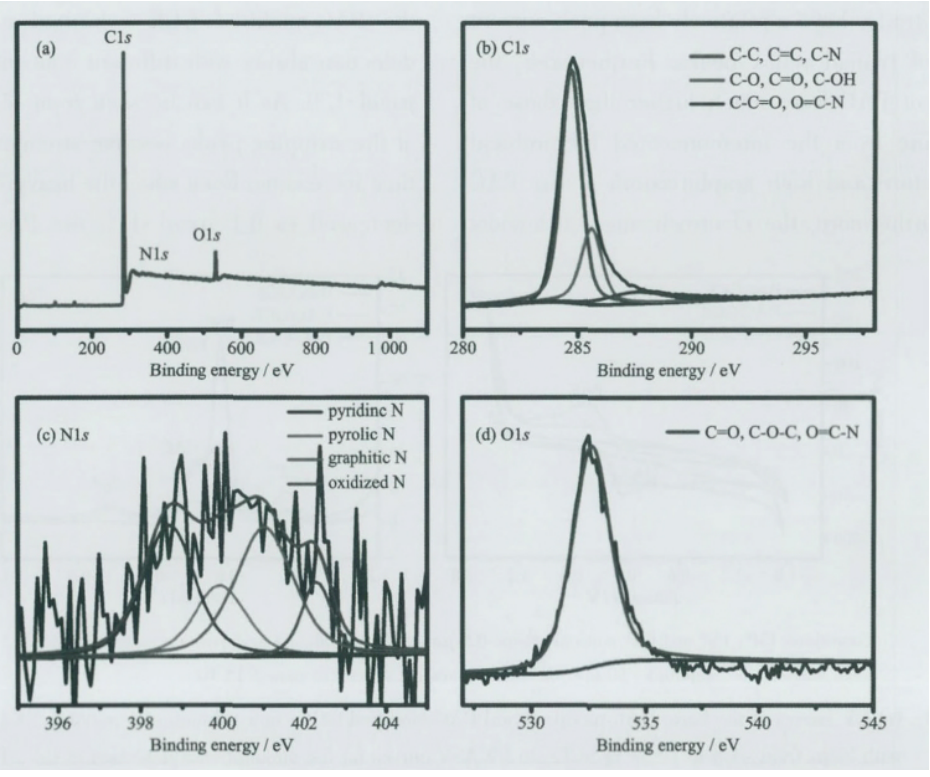

Fig.3　(a) XPS spectra of the (a) surface chemical composition of PAC; (b) C1*s*, (c) N1*s* and (d) O1*s* chemical states

Although the exact role of each nitrogen species during the electrochemical process is still a subject of ongoing research, graphitic-N and pyridinic-N are broadly considered to play a vital role during electrochemical activities. As shown in Fig.3c, the proportions of graphitic and pyridinic were relatively higher than those of oxidized-N and pyrrolic-N, indicating a potentially high electrochemical performance of the present obtained PAC materials. Fig.4d shows the O1*s* peak at 532.6 eV corresponding to binding energy of C=O, O-C-O, O=C-N, which agreed with that of the C peaks[39].

2.3 Electrochemical performance of the PAC modified electrode

A series of CV and SWASV electrochemical experiments were used to investigate the electrochemical properties of the PAC-modified GCE. The conductivity of the different electrodes was investigated using $K_3[Fe(CN)_6]$ as redox probes. Fig.4a demonstrates that the CV curves responses of bare, UAC-modified and PAC-modified GCEs in a solution of 5 mmol·L^{-1} $K_3[Fe(CN)_6]$ with steps from −1.8 to 1.5 V vs SCE. Comparing with the bare electrode, the modified electrodes have a relatively high peak current and a pair of typical redox peaks. Furthermore, the redox peaks of PAC were much higher than those of UAC, resulting from the interconnected hierarchical pore architecture and high graphitization of the PAC materials. Furthermore, the electrochemical behaviors of the PAC-modified GCE towards Cd^{2+}, Pb^{2+} and Cu^{2+} were measured by the SWASV method. Fig.4b shows the SWASV curves of the bare electrode and the modified electrode in a 0.5 μmol·L^{-1} heavy metal ion solution. In contrast with the bare GCE, the modified GCEs both exhibited three typical dissolution peaks corresponding to Cd^{2+}, Pb^{2+} and Cu^{2+}, and a stable baseline. Notably, the PAC-modified GCE indicated the excellent capability of the simultaneous detection of a variety of heavy metal ions. In the present investigations, it is expected that the interconnected three-dimensional-networked porous structure provides active surface area and serve as transport channels to accelerate mass diffusion and significantly promote exchange efficiency. Therefore, it is likely that PAC is suitable for the detection of heavy metal ions and has the potential for widespread application in real-time online and continuous monitoring.

To obtain a higher sensitivity and a lower detection limit for the detection of the three heavy metal ions, the effects of deposition time, deposition potential and heavy ion liquid concentration on the detection were investigated. Fig.5 clearly shows that the PAC-modified GCE exhibited a relatively high detection ability with different concentrations (0.1~1.0 μmol·L^{-1}). As it can be seen from Fig.5a, the signals of the stripping peaks became stronger with deposition time increasing. Even when the heavy ion concentration decreased to 0.1 μmol·L^{-1}, the PAC-modified GCE

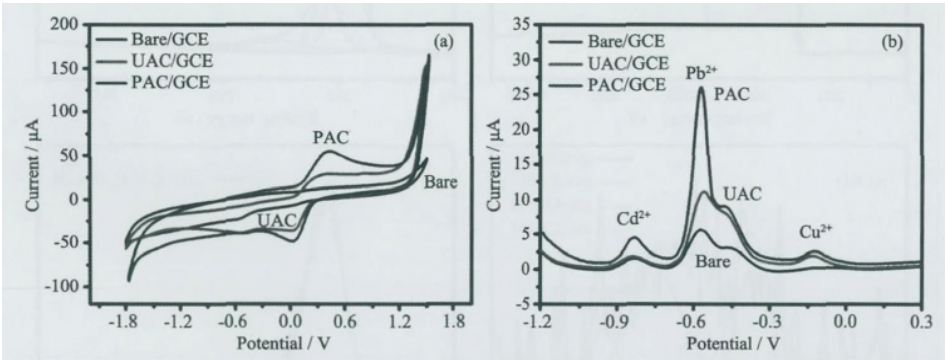

Conditions: Cd^{2+}, Pb^{2+} and Cu^{2+} concentrations: 0.5 μmol·L^{-1}; pH value: 4.8; deposition potential: −2.1 V; room temperature; amplitude: 50 mV; increment potential: 4 mV; frequency: 15 Hz

Fig.4 (a) CV curves of the bare, UAC-modified and PAC-modified GCEs in a solution of 5 mmol·L^{-1} $K_3[Fe(CN)_6]$, with steps from −1.8 to 1.5 V vs SCE; (b) SWASV curves for the simultaneous detection of Cd^{2+}, Pb^{2+} and Cu^{2+} with the modified PAC/GCE, UAC/GCE and bare/GCEs

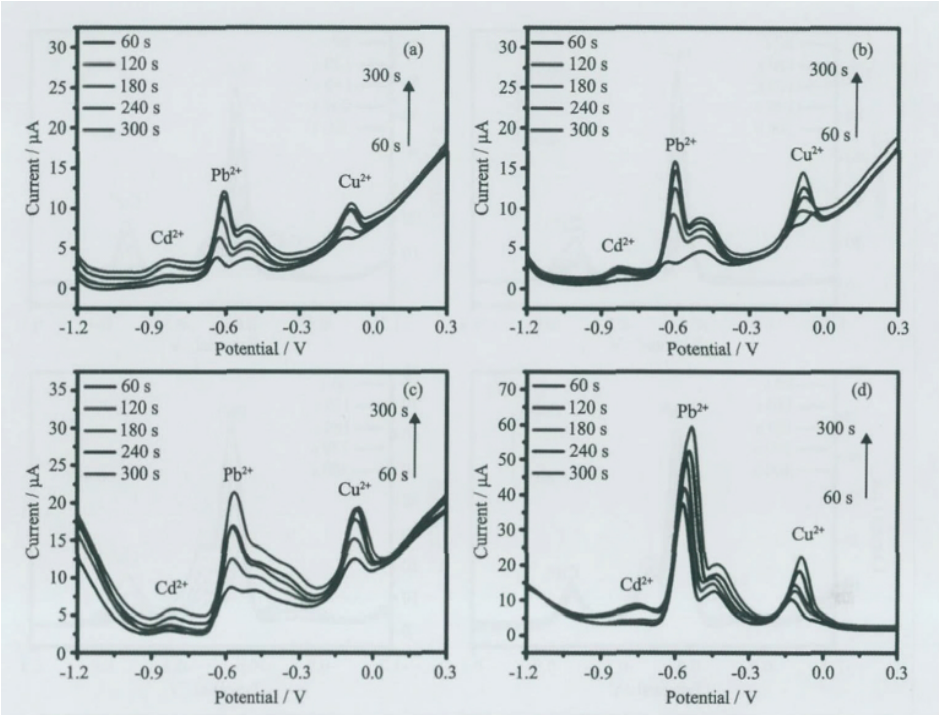

Other experimental conditions were the same as those listed in Fig.4

Fig.5　SWASV curves for the simultaneous detection of Cd^{2+}, Pb^{2+} and Cu^{2+} over a deposition time range from 60~300 s using PAC/GCE at different concentrations of metal ion solution: (a) 0.1, (b) 0.2, (c) 0.5 and (d) 1.0 μmol·L^{-1}

still obtains certain stripping currents and typical stripping peaks. For the simultaneous detection of Cd^{2+}, Pb^{2+} and Cu^{2+} in a 1.0 μmol·L^{-1} metal ion solution, the peak current greatly increased, and the peaks were well separated with a broad range of peak potentials and good peak symmetry. However, for the detection of low concentrations of Cd^{2+}, Pb^{2+} and Cu^{2+} (such as 0.1 and 0.2 μmol·L^{-1}), due to insufficient deposition and dissolution processes, the results indicated that the dissolution peaks are no longer symmetrical and poorly separated. Although the sensitivity at low concentrations decreased, the detection performance was still remarkable because of the use of metal-free electrodes. The results show that the PAC is suitable for detecting Cd^{2+}, Pb^{2+} and Cu^{2+} simultaneously with excellent sensitivity and a low detection limit.

When using SWASV, the sensitivity of the heavy metal ions in the buffer solution was limited by the deposition potential, and thus the effect of deposition potential was investigated. Fig.6 clearly shows higher detection levels of the PAC-modified GCE with the different deposition times (60~300 s) and potentials (−2.4~−1.2 V) at 1.0 μmol·L^{-1}. As shown in Fig.6, the signals of the stripping peaks increased with the deposition potential raising. The detection results show that the PAC materials have excellent ability to adsorb and desorb heavy metal ions. Therefore, the experimental parameters (deposition time and potential) can be further optimized to obtain a higher sensitivity and a lower detection limit.

2.4　Electrochemical experimental parameter optimization of the PAC modified electrode

It is well recognized that the deposition potential plays an important role in ion enrichment, which depends on whether the ion enrichment oxidation and reduction are sufficient or not. Fig.7a shows the influence of the deposition potential, and the results indicated that the stripping currents of Cd^{2+}, Pb^{2+} and Cu^{2+} showed a decreasing trend from −0.9 to −1.8 V and then increased. The ion enrichment was stable at low potentials and thus a deposition potential of −2.1 V was determined as the optimum potential. At this deposition potential, the heavy ions can be reduced at

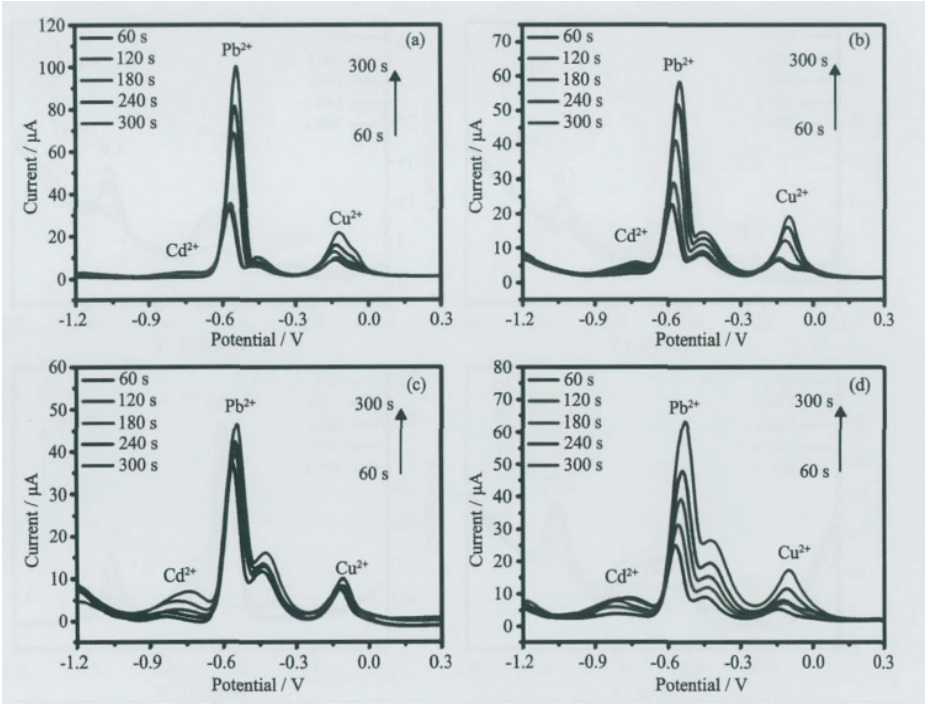

Other experimental conditions were the same as those listed in Fig.4

Fig.6 SWASV curves for the simultaneous detection of 1.0 μmol·L^{-1} Cd^{2+}, Pb^{2+} and Cu^{2+} solutions with different deposition potentials of (a) −1.2, (b) −1.5, (c) −1.8 and (d) −2.4 V

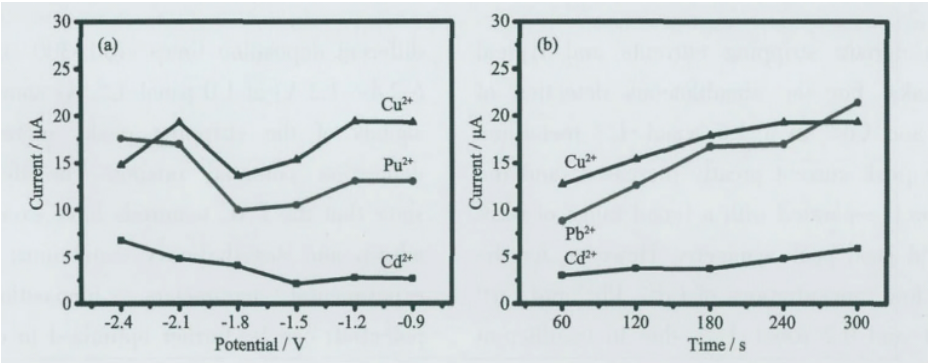

All data were captured using SWASV detection of a metal ion solution containing 0.1 μmol·L^{-1} each of Cd^{2+}, Pb^{2+} and Cu^{2+}; Deposition time tested in Fig.7a was 240 s, and the deposition voltage in Fig.7b was −2.1 V; Other experimental conditions were the same as those in Fig.4

Fig.7 Experimental deposition potential and deposition time optimization

the electrode surface efficiently.

The deposition time affect the concentration of heavy metal ions on the surface of the working electrode. When the deposition time increased, there were more heavy metal ions on the electrode surface for reduction enrichment, and the electrode stripping voltammetry current became higher. However, when the deposition time further increased, the concentration of the heavy metal ions on the surface decreased and thus the dissolution peak current stabilized. Moreover, an excessive extended deposition time lead to an increase in the detection time. As Fig.7b shows, the signals of the stripping peaks continued to rise as the deposition time increased. When the deposition time reached 240 s, the stripping currents of Cu^{2+} began to decline. In conclusion, the deposition time of 240 s is determined to be the optimum time.

To further analyze the linear relationship between the peak current and the ion concentration of heavy metals during the simultaneous detection Cd^{2+}, Pb^{2+}

and Cu^{2+}, SWASV was used to investigate the 0.1~1.0 μmol·L^{-1} Cd^{2+}, Pb^{2+} and Cu^{2+} combined solution under optimal condition, as shown in Fig.8a. The peak current of the dissolution peak went up the increase of the ion concentration. Cd^{2+}, Pb^{2+} and Cu^{2+} were detected at potentials of −0.84, −0.58 and 0.10 V, respectively. To further study the linear relationship among the ions, the relationship between the peak current and the ion concentration was obtained by a linear fitting. Fig.8b, c and d correspond to the linear curves of Cd^{2+}, Pb^{2+} and Cu^{2+}, respectively. It is clearly observed that as the ion concentration increased from 0.1 to 1.0 μmol·L^{-1}, the calibration curve for each ion peak current increased linearly. Specifically, the Cd^{2+} calibration curve equation was y=2.352+22.88x; the Pb^{2+} calibration curve equation was y=7.13+82.37x; and the Cu^{2+} calibration curve equation was y=0.357+34.495x; the correlation coefficients of Cd^{2+}, Pb^{2+} and Cu^{2+} were 0.978, 0.989 5 and 0.999, respectively. All the error bars in the figures were the standard deviations calculated by the three consecutive experiments. The results demonstrated that the detection of heavy metal ions by the PAC-modified electrode was linear. From the calibration curve and the linear correlation coefficient, it can be seen that PAC has a high sensitivity and very good linear range. Therefore, PAC is an ideal electrode material for the detection of heavy metal ions.

Accordingly, the linear range, sensitivity and the relative standard deviations (RSD) for the PAC-modified GCE for the simultaneous detection of these three metal ion species are summarized in Table 1. The linear range of the detection concentration in our experiments was from 0.1~1.0 μmol·L^{-1}. The sensitivity of the PAC-modified GEC for Pb^{2+} was the highest, exhibiting more remarkable electrochemical response and stability. The RSDs of PAC for each ion were measured using 5 replicate experiments, which indicated that the samples can be used to detect heavy metal ions simultaneously with high repeatability. The detection performance of the PAC-modified GCE towards the detection of Cd^{2+}, Pb^{2+} and Cu^{2+} simultaneously at 0.5 μmol·L^{-1} after 7 days of storage in air is displayed in Fig.9a. It is obvious that the

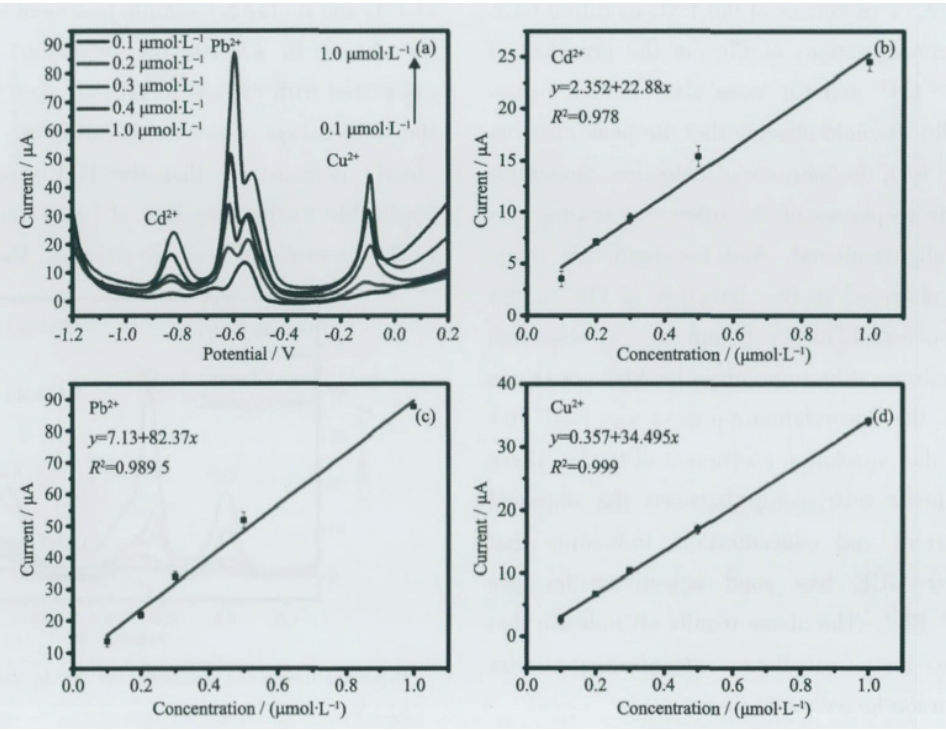

Deposition time tested was 240 s, and the deposition voltage was −2.1 V

Fig.8　(a) SWASV curves for the simultaneous detection of Cd^{2+}, Pb^{2+} and Cu^{2+} at different concentrations; (b~d) Corresponding calibration curve plots for Cd^{2+}, Pb^{2+} and Cu^{2+}

Table 1 Summary of the analytical parameters for the simultaneous detection of heavy metal ions over the PAC-modified GEC

Performance		Linear range / (μmol·L^{-1})	Sensitivity / (μA·μmol^{-1})	RSD at 0.5 μmol·L^{-1} / %
Simultaneous detection	Cd^{2+}	0.1~1.0	22.88	5.41
	Pb^{2+}	0.1~1.0	82.37	9.66
	Cu^{2+}	0.1~1.0	34.495	1.7

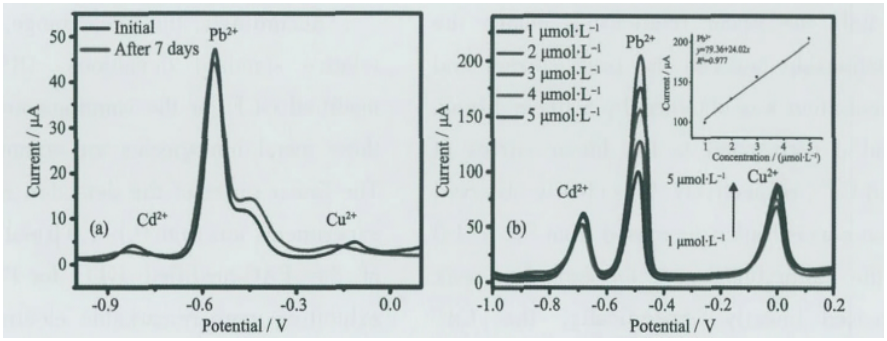

Experimental conditions were the same as those listed in Fig.4

Fig.9 (a) SWASV curves for the simultaneous detection of Cd^{2+}, Pb^{2+} and Cu^{2+} in initial and after 7 days of storage at 0.5 μmol·L^{-1}; (b) Anti-interface experiment and the corresponding calibration plots (Inset) of the PAC-modified GCE for Pb^{2+} detection

stripping currents were nearly constant and remained steady after 7 days, which indicated that the PAC-modified GCE is suitable for practical applications. To further research the interference of the co-existing ions, the SWASV responses of the PAC-modified GCE at different concentrations of Pb^{2+} in the presence of 0.5 μmol·L^{-1} Cd^{2+} and Cu^{2+}were also studied, respectively (Fig.9b). It could observe that the peak currents of Pb^{2+} raised with the increase of detection concentration while the responses of the other co-existing ions were practically unaltered. And no significant interference was observed in the detection of Pb^{2+} under the certain concentrations of Cd^{2+} and Cu^{2+}. As observed, the corresponding calibration curves for Pb^{2+} are shown insert Fig.9b, the linearization equation was y=79.36+24.02x, with the correlation coefficient of 0.977. There is a good linear relationship between the obtained stripping current and concentration, indicating that PAC-modified GCE has good selectivity for the detection of Pb^{2+}. The above results all indicate that the samples have excellent anti-interference for detection of trace heavy metal ions.

2.5 Electrochemical performance in realistic water of the PAC modified electrode

To further evaluate the accuracy of PAC for realistic sample applications, the PAC-modified GCE was used for monitoring Cd^{2+}, Pb^{2+} and Cu^{2+} ions in a real water sample. A realistic water sample was diluted with an HAc-NaAc (pH=4.8) buffer solution at a ratio of 1∶1, and no further sample treatment was conducted. As shown in Fig.10, the oxidation peak currents associated with various metal ions were increased with the increasing of ion concentration. These results clearly demonstrate that the PAC-modified GCE is applicable to the detection of heavy metal ions, even in the presence of realistic samples. Recovery experi-

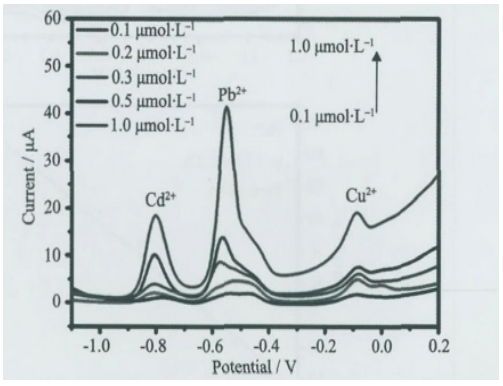

Deposition time tested was 240 s, and the deposition voltage was −2.1 V

Fig.10 SWASV curves for the simultaneous detection of Cd^{2+}, Pb^{2+} and Cu^{2+} in different concentrations in a realistic water sample

ments were performed to further guarantee the repeatability of the SWASV for the analysis of Cd^{2+}, Pb^{2+} and Cu^{2+} in realistic samples. As shown in Table 2, the got recoveries were between 88.7% and 106.8%, revealing that PAC-modified GCE possesses great potential capability for practical applications.

In the present investigations, metal-free carbon materials can be easily obtained by a facile chemical activation and pyrolysis process from inexpensive and readily available pomelo peels. The interconnected micropores and mesopores act as efficient ion-transfer channels and provide active surface areas with high accessibility, which serve as transport highways to accelerate mass diffusion and promote exchange efficiency significantly. The high degree of graphitization of the carbon materials further enhances the electroanalytical activity by accelerating the electron transfer. Consequently, the metal-free biomass-derived carbon materials exhibit excellent sensitivity with a low detection limit for heavy metal detection.

Table 2　Recovery experiments for electroanalysis of Cd^{2+}, Pb^{2+} and Cu^{2+} in realistic samples using SWASV

	Added concentration / ($\mu mol \cdot L^{-1}$)	Found concentration / ($\mu mol \cdot L^{-1}$)	Recovery / %	RSD / %
Cd^{2+}	0.1	0.103 9	103.9	2.7
	0.2	0.178 5	89.3	8.0
	0.3	0.277 0	92.3	5.6
	0.5	0.530 9	106.2	4.2
	1.0	0.982 6	98.3	1.2
Pb^{2+}	0.1	0.105 4	105.4	3.7
	0.2	0.198 2	99.1	0.6
	0.3	0.320 5	106.8	1.4
	0.5	0.487 0	97.4	1.8
	1.0	1.008 4	100.8	0.6
Cu^{2+}	0.1	0.088 7	88.7	8.4
	0.2	0.200 1	100.05	0.03
	0.3	0.309 3	103.1	2.1
	0.5	0.500 1	100.02	0.03
	1.0	0.996 3	99.63	0.26

3　Conclusions

Herein, we demonstrated a facile method for the highly sensitive simultaneous detection of Cd^{2+}, Pb^{2+} and Cu^{2+} with free-metal porous biomass-derived carbon materials. The honeycomb-like carbon materials were obtained by a facile KOH activation and pyrolysis process from inexpensive and readily available pomelo peels with a high specific surface area of 1 055 $m^2 \cdot g^{-1}$ and a high degree of graphitization. The porous carbon materials were utilized for heavy metal ion detection, and the results indicate that the PAC electrode exhibits high sensitivity, excellent stability and repeatability and a low detection limit for the simultaneous detection of Cd^{2+}, Pb^{2+} and Cu^{2+}. The interconnected micropores and mesopores act as efficient ion-transfer channels and provide active surface areas with high accessibility, which serve as transport highways to accelerate mass diffusion and significantly promote exchange efficiency. This work demonstrates a promising and appealing method for the fabrication of porous carbon materials from biomass materials and their application in electrochemical-related fields.

Acknowledgements: This study was supported by the National Natural Science Foundation of China (NSFC) (Grant No.51373154, 51573166).

References:

[1] Gumpu M B, Sethuraman S, Krishnan U M, et al. *Sens. Actuators B*, **2015**,**213**:515-533

[2] Bansod B, Kumar T, Thakur R, et al. *Biosens. Bioelectron.*,

2017,**94**:443-455
[3] Aragay G, Merkoi A. *Electrochim. Acta*, **2012**,**84**:49-61
[4] Fakhre N A, Ibrahim B M. *J. Hazard. Mater.*, **2018**,**343**:324-331
[5] March G, Nguyen T D, Piro B. *Biosensors*, **2015**,**5**:241-275
[6] Aranda P R, Pacheco P H, Olsina R A, et al. *J. Anal. At. Spectrom.*, **2009**,**24**:1441-1445
[7] Silva E L, Roldan P S, Gine M F. *J. Hazard. Mater.*, **2009**, **171**:1133-1138
[8] Pohl P. *TrAC Trends Anal. Chem.*, **2009**,**28**:117-128
[9] Sawczak M, Kamińska A, Rabczuk G, et al. *Appl. Surf. Sci.*, **2009**,**255**:5542-5545
[10]Priyadarshini E, Pradhan N. *Sens. Actuators B*, **2017**,**238**: 888-902
[11]Li S, Xu L G, Ma W, et al. *Small*, **2015**,**11**:3435-3439
[12]Jamali M R, Assadi Y, Shemirani F, et al. *Anal. Chim. Acta*, **2006**,**579**:68-73
[13]Meucci V, Laschi S, Minunni M, et al. *Talanta*, **2009**,**77**: 1143-1148
[14]Alves G M S, Rocha L S, Soares H. *Talanta*, **2017**,**175**:53-68
[15]Gao C, Yu X Y, Xiong S Q, et al. *Anal. Chem.*, **2013**,**85**: 2673-2680
[16]Wei Y, Gao C, Meng F L, et al. *J. Phys. Chem. C*, **2011**,**116**: 1034-1041
[17]Cui L, Wu J, Ju H X. *Biosens. Bioelectron.*, **2015**,**63**:276-286
[18]Jin H Y, Wang J, Su D F, et al. *J. Am. Chem. Soc.*, **2015**,**137**: 2688-2694
[19]Ratso S, Kruusenberg I, Käärik M, et al. *Carbon*, **2017**,**113**: 159-169
[20]Zhu H, Gu L, Yu D N, et al. *Energy Environ. Sci.*, **2017**,**10**: 321-330
[21]Hu C G, Dai L M. *Adv. Mater.*, **2017**,**29**:1-9
[22]Xin W, Song Y H, Peng J F, et al. *ACS Sustainable Chem. Eng.*, **2017**,**5**:2312-2319
[23]Goldfarb J L, Dou G, Salari M, et al. *ACS Sustainable Chem. Eng.*, **2017**,**5**:3046-3054
[24]Zang Y P, Zhang H M, Zhang X, et al. *Nano Res.*, **2016**,**9**: 2123-2137
[25]Wang J C, Kaskel S. *J. Mater. Chem.*, **2012**,**22**:23710-23725
[26]Tay T, Ucar S, Karagoz S. *J. Hazard. Mater.*, **2009**,**165**:481-485
[27]Lee J, Kim J, Hyeon T. *Adv. Mater.*, **2006**,**18**:2073-2094
[28]Dias J M, Alvim-Ferraz M C, Almeida M F, et al. *J. Environ. Manage.*, **2007**,**85**:833-846
[29]Liang C D, Li Z J, Dai S. *Angew. Chem. Int. Ed.*, **2008**,**47**: 3696-3717
[30]Wang H, Yin F X, Chen B H, et al. *Appl. Catal. B*, **2017**, **205**:55-67
[31]Qu G, Jia S F, Wang H, et al. *ACS Appl. Mater. Interfaces*, **2016**,**8**:20822-20830
[32]Hong K L, Qie L, Zeng R, et al. *J. Mater. Chem. A*, **2014**,**2**: 12733-12738
[33]Yao S S, Zhi L F, Guo J, et al. *Int. J. Electrochem. Sci.*, **2018**,**13**:542-550
[34]Sudhan N, Subramani K, Karnan M, et al. *Energy Fuels*, **2017**,**31**:977-985
[35]Wang H, Min S X, Ma C, et al. *Nat. Commun.*, **2017**,**8**:13592
[36]Zhang B, Chen J D, Zhu H, et al. *Electrochim. Acta*, **2016**, **196**:422-430
[37]Long C L, Chen X, Jiang L L, et al. *Nano Energy*, **2015**,**12**: 141-151
[38]Wang H L, Xu Z W, Kohandehghan A, et al. *ACS Nano*, **2013**,**7**:5131-5141
[39]Li H Z, Sun Z B, Zhang L, et al. *Colloids Surf. A*, **2016**,**489**: 191-199